Field-effect plasmonic transistors based on metallic-semiconducting carbon nanotube junctions

Yufeng Xie[1], Kunqi Xu[1], Zhenghan Wu[1], Cheng Hu[1], Saiqun Ma[1], Xianliang Zhou[1], Zhichun Zhang[1], Peiyue Shen[1], Yi Chen[1], Chengjia Zhang[1], Liguo Wang[1], Kenji Watanabe[2], Takashi Taniguchi[3], Qi Liang[1], Guibai Xie[1], Seojoo Lee[4], Ji-Hun Kang[5,6]*, Zhiwen Shi[1,7,8]*

[1]Key Laboratory of Artificial Structures and Quantum Control (Ministry of Education), School of Physics and Astronomy and Tsung-Dao Lee Institute, Shanghai Jiao Tong University, Shanghai 200240, China.

[2]Research Center for Electronic and Optical Materials, National Institute for Materials Science, 1-1 Namiki, Tsukuba 305-0044, Japan.

[3]Research Center for Materials Nanoarchitectonics, National Institute for Materials Science, 1-1 Namiki, Tsukuba 305-0044, Japan.

[4]School of Applied and Engineering Physics, Cornell University, Ithaca, NY 13853, USA

[5]Department of Optical Engineering, Kongju National University, Cheonan 31080, Republic of Korea.

[6]Department of Future Convergence Engineering, Kongju National University, Cheonan 31080, Republic of Korea.

[7]Collaborative Innovation Centre of Advanced Microstructures, Nanjing University, Nanjing 210093, China.

[8]State Key Laboratory of Micro-Nano Engineering Science, Shanghai Jiao Tong University, 800 Dongchuan Road, Shanghai 200240, China

*To whom correspondence should be addressed: jihunkang@kongju.ac.kr, zwshi@sjtu.edu.cn

Abstract: Nanophotonic circuits are regarded as a transformative technology that can overcome many challenges faced by electronic circuits, particularly concerning the operating frequency limits. However, the development of nanophotonic circuits utilizing plasmons is strongly hampered by the absence of fundamental building blocks, such as long-lived deep-subwavelength plasmons, plasmonic waveguides, and field-effect plasmonic transistors (FEPTs). Here, we demonstrate Luttinger-liquid FEPTs based on metallic-semiconducting carbon nanotube junctions. In these devices, the propagation of plasmon waves across the junction can be efficiently controlled through electrostatic gating. Theoretical analysis and numerical simulations indicate that the reflection/transmission of Luttinger-liquid plasmons at junctions can be well captured by the Fresnel equation. This result suggests that the classical Fresnel law persists for Luttinger-liquid plasmons with reduced dimensionality. Our study not only uncovers the fundamental propagation characteristics of Luttinger-liquid plasmons at junctions, but also introduces a new category of FEPTs that could facilitate the development of high-frequency nanophotonic circuits.

Keywords: Carbon nanotube, Plasmonics, Near-field infrared nanoscopy, Luttinger liquid, Plasmonic

transistor.

With the rapid advancement of communication technology, there is a growing demand for faster devices and improved chip integration. Current electronic circuits are struggling to meet the high-speed operation requirements, which has prompted researchers to explore photonic circuits as an effective solution. Photonic circuits offer significant advantages over traditional electronic systems, not only in operating speed and bandwidth, but also in energy efficiency and heat generation[1-8]. However, the miniaturization of essential components in photonic circuits is challenging due to the diffraction limit of light, which strongly hampers the integration of these circuits. Plasmons—hybrid quasiparticles formed from the coupling of electrons and photons—exhibit photon-like frequencies and electron-like wavelengths, making them a promising link between electronic and photonic circuits. In particular, plasmons in low-dimensional materials are recognized for their ability to manipulate light-matter interactions at deep sub-wavelength scales, making them suitable for next-generation nanophotonic circuits[9-18]. To date, substantial progress has been made in the development of plasmonic-based photonic devices, including waveguides[19-24], gain units[25, 26], modulator[27-29] and detectors[30, 31]. However, while field-effect transistors (FETs) are crucial components in electronic circuits, their nanophotonic counterpart, the field-effect plasmonic transistors (FEPTs), remain underdeveloped.

Here, we report on the design and demonstration of gate-tunable FEPT devices based on carbon nanotube (CNT) junctions featuring both metallic and semiconducting sections. In these devices, plasmons propagate within the metallic section but are blocked in the semiconducting section if the Fermi level resides within the band gap, representing the off state of the FEPT. By applying a gate voltage, the semiconducting region can be tuned to become optically conductive, enabling plasmon propagation across the junction and transitioning the device to the on state. Using near-field infrared nanoscopy, we experimentally observed the gate-tunable reflection/transmission of one-dimensional (1D) Luttinger-liquid plasmons at the metallic-semiconducting (m-s) junctions. Furthermore, we conducted a rigorous theoretical analysis and performed numerical simulations to investigate the reflection/transmission characteristics of the 1D Luttinger-liquid plasmons at nanoscale junctions. We found that the classical Fresnel equation provides a surprisingly accurate description of the plasmon reflection, indicating its applicability and accuracy at around 1 nm length scale. These findings are pivotal for advancing nanoscale plasmonic circuits.

Single-walled CNTs utilized in this study are grown on hexagonal boron nitride (hBN) flakes on SiO_2/Si chips through chemical vapor deposition (CVD). hBN is selected as the substrate because it is atomically flat and exceptionally clean, which facilitates the observation of plasmons in CNTs. Furthermore, at the excitation wavelength of 10.6 μm utilized in our experiment, hBN exhibits minimal and nearly constant permittivity, showing little response to the incident light. We probe the plasmons in CNTs using a home-made scanning near-field optical microscope (SNOM), the schematic of which is illustrated in Fig. 1a (see more details in SI). A gold-coated atomic force microscope (AFM) tip, illuminated by an infrared light beam, provides momentum compensation and initiates the launch of plasmons in CNTs. The launched plasmons propagate along the nanotube and are reflected back at the end, resulting in interference fringe patterns. The reflected plasmon waves alter the local field beneath the tip as well as the scattered signal, which is recorded by a mercury cadmium telluride (MCT) detector located in the far field. Simultaneously, AFM topography images are captured alongside the near-field infrared images.

Plasmons in CNTs, known as Luttinger-liquid plasmons, exhibit remarkable spatial confinement and a high-quality factor, making them promising candidates for highly integrated plasmonic waveguides and nanophotonic circuits[23, 24, 32, 33]. It is important to note that metallic CNTs consistently support plasmon propagation, whereas in semiconducting CNTs, plasmons can only be observed when the Fermi level is positioned outside the energy gap, which can be controlled using electrostatic gates. Furthermore, due to the different energy band structures near the charge neutral point (CNP), plasmons in metallic CNTs exhibit linear Luttinger-liquid behavior, while those in semiconducting CNTs display non-linear characteristics. The linear dispersion in metallic CNTs results in a constant Fermi velocity, leading to a consistent plasmon wavelength independent of carrier concentration, in contrast to the non-linear dispersion seen in semiconducting CNTs with a gate-dependent plasmon wavelength. Fig.1b presents the extracted plasmon wavelengths of a metallic nanotube under different gate voltages. The inset shows the corresponding near-field infrared images of the nanotube from which wavelengths are extracted. It is evident that the plasmon wavelength in the metallic tube remains constant ($\approx$90 nm) regardless of the gate voltage. On the contrary, plasmon wavelength in the semiconducting tube varies with the gate voltage, as illustrated in Fig. 1c. The dots represent the wavelengths extracted from the near-field images shown in the inset while the blue line represents the predictions made by the nonlinear Luttinger-liquid theory (see detailed linear and nonlinear Luttinger-liquid theory of CNT plasmons in the Supporting Information). The plasmon characteristics observed here align well with findings in previously published literatures[23, 24].

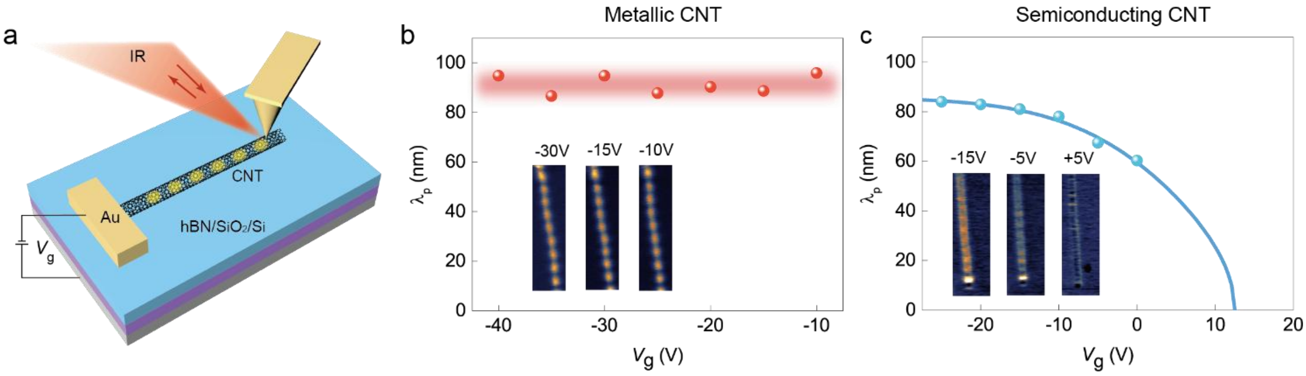

Figure 1. Characteristics of Luttinger-liquid plasmons in metallic and semiconducting carbon nanotubes (CNTs). (a) Schematic of infrared nano-imaging of plasmons in CNTs with electrostatic gating. (b) Gate-independent plasmon wavelength in metallic CNTs. The insets show the infrared nano-imaging of plasmons under different gate voltages. (c) Gate-dependent plasmon wavelength in semiconducting CNTs. Blue dots: experimental data. Blue line: predictions made by nonlinear Luttinger-liquid theory.

Based on the results discussed above, we can develop a FEPT device that incorporates a single CNT with both metallic and semiconducting sections, along with a junction connecting them. The propagation of plasmons through this junction is determined by the carrier concentration in the semiconducting section. Moreover, the distinct plasmon behaviors in the metallic and semiconducting tubes allow for the adjustment of the transmission ratio. To experimentally realize the proposed FEPT structure, we created m-s CNT junctions using temperature-mediated CVD growth. It has been observed that altering the growth temperature affects the diameter of the CNTs: higher temperatures yield thinner tubes, while lower temperatures result in thicker ones[34, 35]. Since the diameter of a CNT is related to its chirality, which in turn affects its conductance[36, 37], we can produce m-s CNT junctions through this approach. In our experiments, we adjusted the temperature from 850°C to 800°C during the growth process to intentionally create CNT segments with different diameters (see more details in SI Figure S1). As a result, we obtained a range of CNT junctions (m-s, m-s-m, s-m-s), as shown in Fig.

S2.

To demonstrate the concept of the FEPT, we fabricated the CNT junctions into a back-gate device and applied a gate voltage between the nanotube and the underlying silicon layer to tune the charge concentration in the CNTs. Simultaneously, SNOM was used to excite and probe the plasmon propagation along the CNTs. Regarding the initial doping state of the FEPT, the Fermi surface lies in the energy gap of the semiconducting section and the CNP of metallic section, as illustrated in Fig. 2a. It is important to note that there are no free charge carriers in the semiconducting section; only the metallic section of the tube allows for plasmon propagation, keeping the FEPT in the off state. When a significant electrostatic gate voltage V_g is applied between the silicon substrate and the tube, the carrier density will either increase or decrease, enabling the semiconducting section to support plasmons, thus turning the FEPT on, as illustrated in Fig. 2b. The near-field infrared images of the FEPT in both off and on states are presented in Figs. 2c and 2d, respectively. Initially, plasmon waves travelling along the metallic section are blocked at the junction point, but they can pass through once the switch is activated.

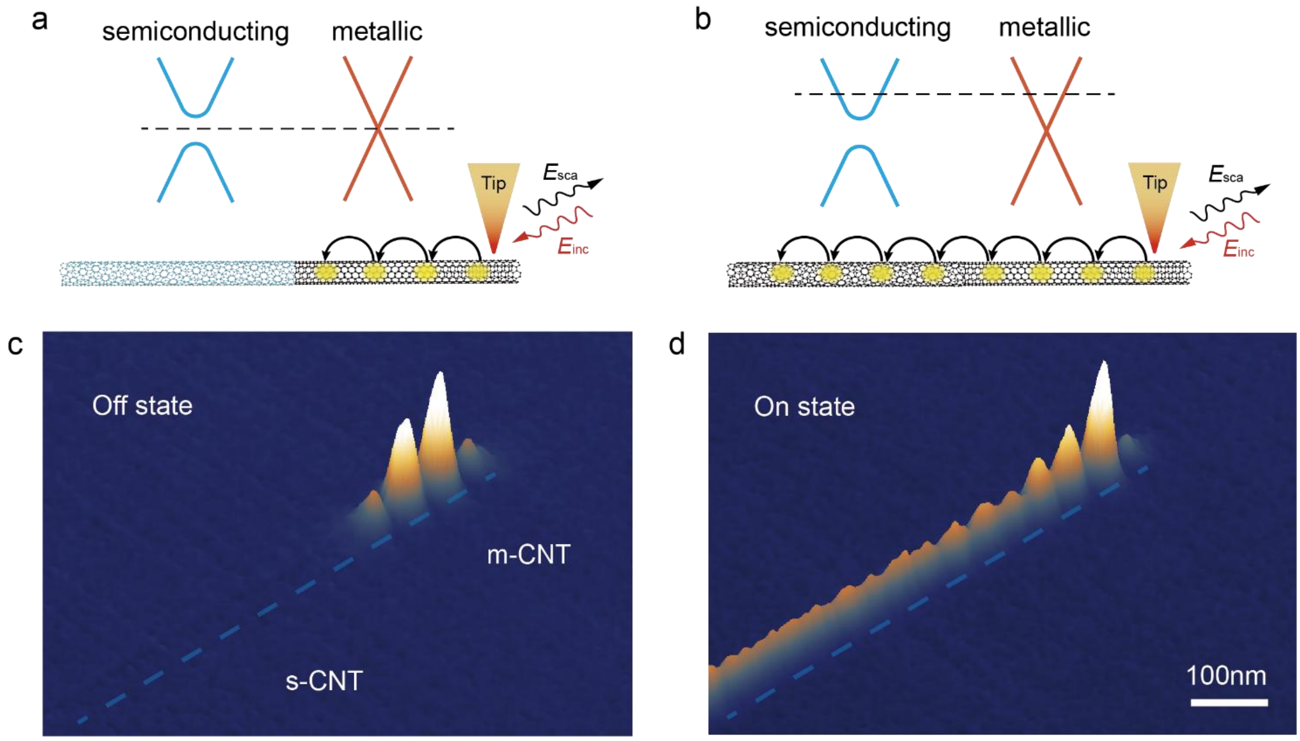

Figure 2. The design of field-effect plasmonic transistors (FEPTs). (a, b) Design of an FEPT based on CNTs with a metallic-semiconducting junction. Schematic of the off-state (a) and the on-state (b) of the FEPT. The insets show the band structures and the Fermi levels at different states of the FEPT. The black dashed lines denote the Fermi levels. (c, d) Infrared nano-imaging of the off-state (c) and the

on-state (d) of an FEPT. The blue dashed lines denote the location of the CNT.

The distinct plasmon behaviors in the metallic and the semiconducting tubes enable the adjustment of plasmon transmission and reflection ratio in the FEPTs. Figure 3 provides a detailed characterization of propagation of plasmon in our devices. Figure 3a presents an AFM topography image of a CNT junction, with an inset showing the height profile of our remarkably small FEPT, which has a channel diameter of only 2.3 nm. The near-field images corresponding to this CNT are shown in Fig. 3b, illustrating the off, ajar, and on states, respectively. In the off state, plasmon waves are blocked at the junction, resulting in an interference-enhanced peak in the line profile. When a gate voltage is applied to the FEPT, plasmon waves can partially travel into the semiconducting section, resembling the behavior of the ajar state. Once the gate voltage reaches a sufficient level, the FEPT is fully activated, allowing plasmon waves to move freely. This leads to a nearly uniform plasmon state on both sides of the junction, indicating a transmission coefficient approaching unity. The plasmon line profiles for the off and the on state from Fig. 3b are extracted and plotted in Fig. 3d. Notably, in the off state, due to nearly complete reflection at the junction, plasmons resonate within the metallic region, resulting in significant enhancement of interference peaks. Conversely, in the on state, the interference fringes diminish due to the increased transmission. To further explore how the transmission coefficient varies with gate voltage, we adjust the electrostatic gate voltage and record the resulting changes in the plasmon line profile, which are plotted in Fig. 3e. Interestingly, the interference-enhanced peak at the junction gradually diminishes as the gate voltage increases, indicating a reduction in plasmon reflection. As mentioned earlier, a higher gate voltage leads to a longer plasmon wavelength in the semiconducting tube. These observations support our general understanding that a larger mismatch in wavelength typically results in an increased reflection.

The results from numerical simulations confirm this trend, as shown in Fig. 3c. We employ the finite element method (COMSOL Multiphysics) to simulate the plasmon propagation and transmission in our FEPTs (see more details in SI). An electronic dipole is positioned at the terminal of the metallic section to serve as a source for plasmon excitation. The launched plasmon waves travel from the metallic region to the semiconducting region, and we observed that the plasmon transmission varies when the permittivity of the metallic section remains constant while that of the semiconducting section is varied. When the permittivity of the semiconducting section is positive (e.g., similar to that of the air), plasmon propagation is forbidden in semiconducting region, resulting a plasmon reflection at the junction, which produces noticeable interference fringes on the metallic section. By varying the permittivity from the positive value to a negative value, the plasmon waves can partially transmit into the semiconducting region, leading to a weaker interference fringe in the metallic section, corresponding to the ajar state. Complete transmission of plasmon waves occurs only when the permittivity (or plasmon wavelength) in both sections is equal. Experimentally, the permittivity and the plasmon wavelength of the semiconducting section can be efficiently tuned by the gate voltage V_g. Both experimental and simulation results align well, demonstrating that an increase in the gate voltage (or carrier density) of the semiconducting section enhances plasmon transmission. Based on these findings, our FEPT design is highly effective, achieving nearly complete transmission in the on state and offering a wide range of gate-tunable transmission.

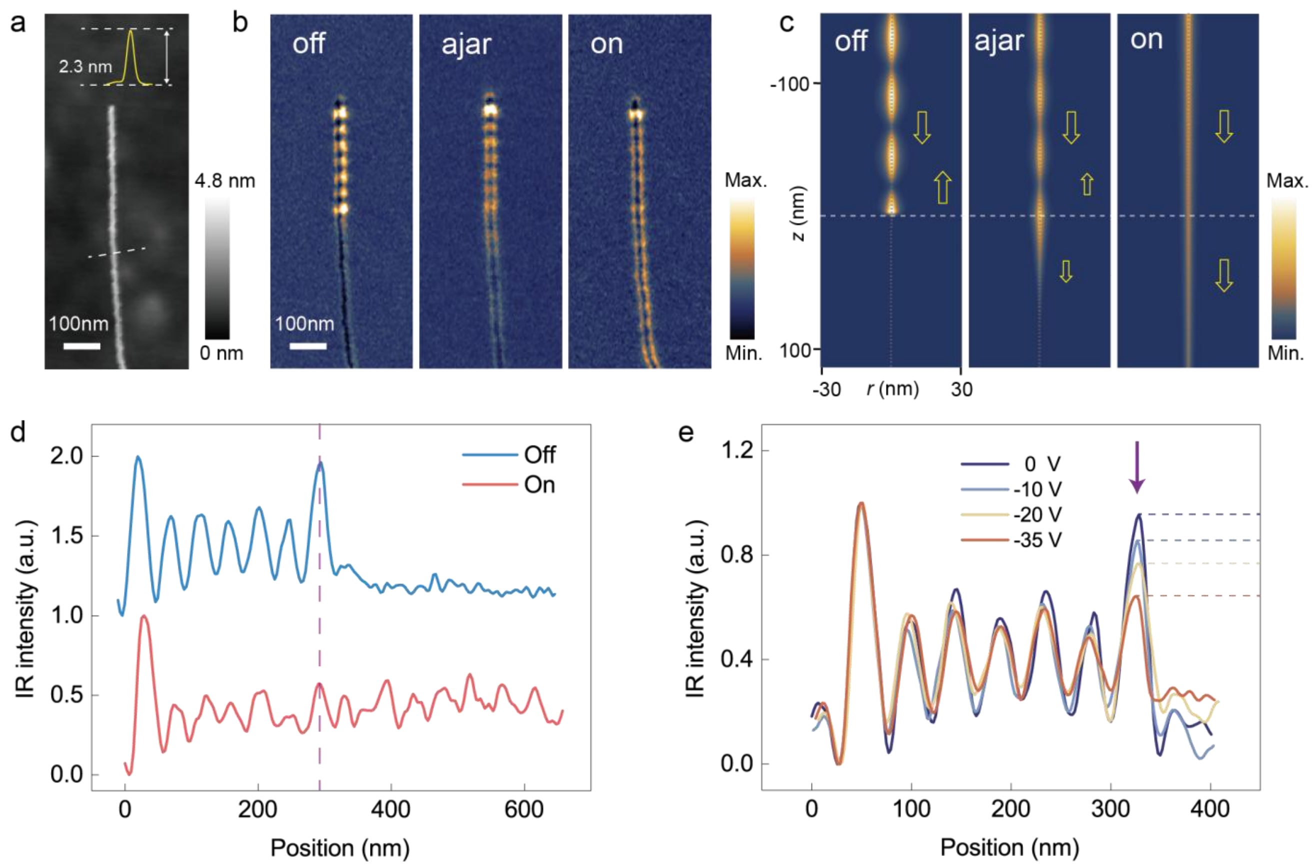

Figure 3. Gate-tunable 1D plasmon propagation across a metallic-semiconducting junction. (a) AFM topography of the FEPT with a tube diameter of 2.3 nm. (b) Infrared nano-imaging of the off-state, ajar-state, and on-state of the FEPT. (c) Numerical simulation of the off, ajar and on states of the FEPT. (d) The extracted plasmon line profiles for the off-state (blue line) and the on-state (red line). (e) The extracted plasmon line profiles of the metallic part of the FEPT under different gate voltages. The purple arrow denotes the junction point.

Due to the absence of wavelength tunability on the metallic side, we propose an improved FEPT design that allows for tunable wavelength control on both sides. The new design, illustrated in the inset of Fig. 4a, includes an m-s junction tube combined with an additional semiconducting tube, resulting in an FEPT made up of two nanotubes. On one side of the junction, there is a metallic tube alongside a semiconducting tube (region 1), while the other side consists of two semiconducting tubes (region 2). In region 1, the plasmon in the metallic tube interacts with that in the semiconducting tube, allowing the wavelength tunability of the semiconducting tube to influence the coupled mode. Figures 4a-f illustrate how plasmon waves progressively travel through the junction as the electrostatic gate voltage increases. The plasmon reflection interference fringes gradually fade on the region 1 side of the junction, while region 2 becomes increasingly illuminated. The reflections extracted from Fig. 4a-f are plotted in Fig. 4h. Notably, the plasmon wavelength of region 1 also increase with V_g, rising from 85 nm to 120 nm, as shown in Fig. 4g. A previous study[23] has reported that the number of plasmon-conducting channels determines the plasmon wavelength, with the ratio of the plasmon wavelength in a CNT bundle to that in a single CNT being $\sqrt{N}$, where *N* is the number of CNTs in the bundle. Given that the ratio of charge neutral and heavily doped states plasmon wavelength of region 1 is approximately $\sqrt{2}$, this supports the presence of two bundled tubes. Moreover, since the range of plasmon wavelength of a single CNT is quite narrow, an FEPT with multiple CNTs can extend this wavelength range, thereby enabling the modulation of the plasmon wavelength and transmission over a wider range (from λ_p to $\sqrt{N}\lambda_p$, where λ_p is the plasmon wavelength of a single CNT). This approach holds promise for engineering diverse structural FEPTs to meet various requirements. Furthermore, achieving local doping within the nanotubes would enable independent tunability of the plasmon wavelength on both sides.

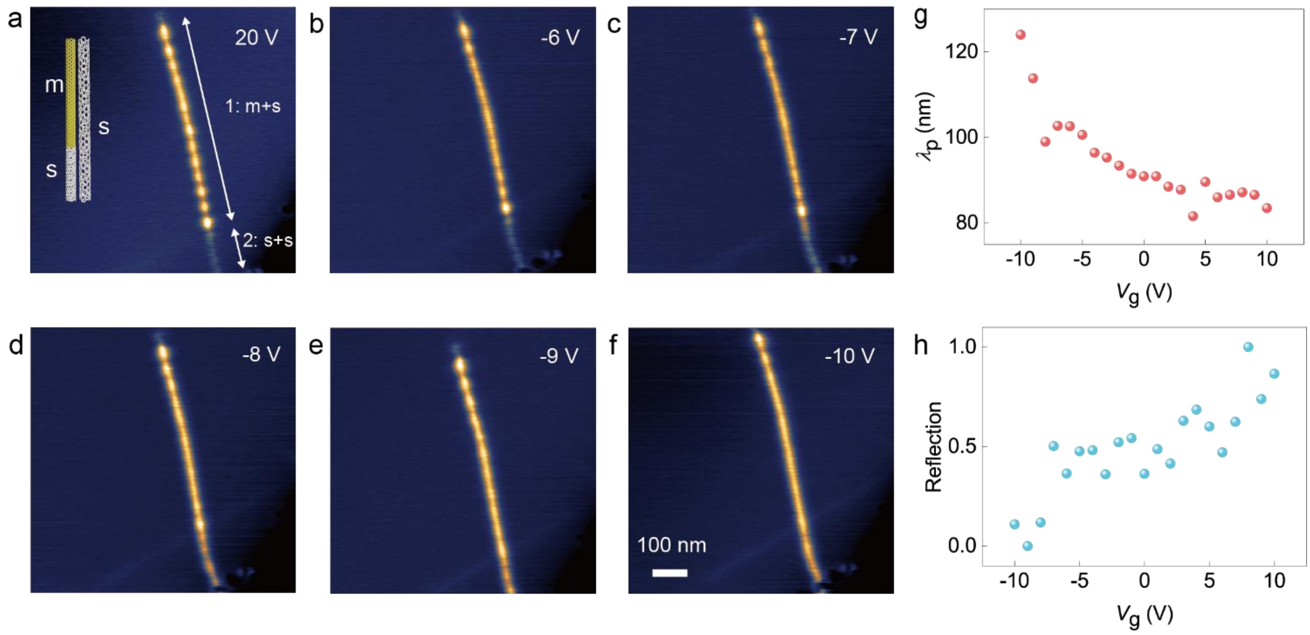

Figure 4. A gate-tunable FEPT in a bundled CNT junction. (a-f) Infrared nano-imaging of the FEPT under different gate voltages. With applying a more negative gate voltage, the plasmon interference fringes near the junction gradually disappear, indicating an increase of plasmon transmission and decrease of reflection. The inset in (a) show the structure of the bundled CNT junction. (g) Plasmon wavelength of the metallic-like section as a function of the gate voltage. (h) The reflection of plasmons as a function of the gate voltage.

To theoretically understand the 1D plasmon reflection behavior at junctions in our FEPTs, we developed a rigorous analytic model based on the Maxwell's equation and the coupled mode theory. We employ the cylindrical coordinates (r, φ, z), and position the axis of the CNT along the z-axis. A junction is located at $z = 0$, which divides the CNT into two sections, allowing the incident plasmons to propagate from the left section (region 1) to the right section (region 2). We represent the 1D plasmons as the lowest-order cylindrical surface-bound waves with no azimuthal dependency. Notably, electromagnetic waves in this system should be expressed as the propagation 1D plasmon mode $|p_s\rangle$ together with the radiation modes $|u_{q,s}\rangle$, which are orthogonal eigenmodes. When the incident 1D plasmons reach the junction, they couple not only to the reflected and transmitted 1D plasmons in regions 1 and 2, respectively, but also to the radiation modes in the proximity of the junction. We note that this coupling to the radiation modes is essential, because the boundary conditions at the junctions, required by the Maxwell's equation, cannot be satisfied without the radiation modes. By considering all these procedure, we can express the complete φ-component of magnetic fields in regions 1 and 2, respectively, as $\left|H_{\varphi,1}(z)\right\rangle = \left(e^{ik_{z,1}z} - Re^{-ik_{z,1}z}\right)|p_1\rangle - \int_0^\infty dq\alpha_q \left|u_{q,1}\right\rangle e^{-i\sqrt{k_0^2-q^2}z}$, and $\left|H_{\varphi,2}(z)\right\rangle = Te^{ik_{z,2}z}|p_2\rangle + \int_0^\infty dq\beta_q \left|u_{q,2}\right\rangle e^{i\sqrt{k_0^2-q^2}z}$, where R and T are the reflection and transmission coefficients, $k_{z,s}$ is the momentum of $|p_s\rangle$ in the z-direction, q is the momentum of the radiation modes in the r-direction, k_0 the free-space photon momentum, and α_q and β_q are amplitudes of the radiation modes in the region 1 and 2, respectively. The corresponding r-component of the electric fields can be readily derived from the magnetic field. Then, by applying the boundary conditions at the junctions, which correspond to the continuity of the tangential components of the electric and magnetic fields, we obtained four coupled integral equations. After that, we quantized the radiation mode as an approximation and attained the R and T as, $R = \frac{W_1-(W_2+W_3)}{W_1+(W_2+W_3)}$, and $T = \frac{2W_1W_2}{W_1+(W_2+W_3)}$, where $W_{1,2,3}$ are the dimensionless coupling strengths (see Supporting Information for details). The obtained reflection coefficients align very well with the Fresnel equation, as shown in Fig. 5b.

To check the validity of our analytic theory, we further conducted numerical simulations. We first recreated the phenomena that 1D plasmon propagated along the CNT junction and transmitted from metallic part to semiconducting part without loss by solving Maxwell's equations by using the finite-difference time-domain (FDTD) method. Shown in Fig. 5a are numerically calculated field maps of 1D plasmon amplitudes. The reflection of 1D plasmons at junctions for both $\lambda_{inc} > \lambda_{trans}$ and $\lambda_{inc} < \lambda_{trans}$ cases are well demonstrated in the form of fringes from constructive/destructive interferences between incident and reflected 1D plasmons. The reflection amplitudes under different wavelength mismatch are extracted from the electric field amplitude near CNT surface. As shown in Fig. 5b, our analytical and numerical results show remarkable consistency, while experimental data also fit well with them. More interestingly, we can see that the amplitudes of the reflection coefficients from all results agree with those based on the Fresnel equations given by

$$R_{Fresnel} = \frac{Z_{trans}^{sp} - Z_{inc}^{sp}}{Z_{trans}^{sp} + Z_{inc}^{sp}} = \frac{k_{trans} - k_{inc}}{k_{trans} + k_{inc}}$$

where Z_{inc}^{sp}, k_{inc} and Z_{trans}^{sp}, k_{trans} are the wave impedances and propagating momenta of 1D plasmons in the incident (metallic) and transmitting (semiconducting) regions, respectively. Based on this, we propose that the classical Fresnel law remains applicable to the transmission behavior of 1D plasmons, further indicating its universality in nanophotonics. While further theoretical and experimental studies are still required for a better quantitative understanding, our results demonstrate that the transmission of 1D plasmons can be controlled through wavelength matching. Our findings may open new avenues for tunable transmission elements and provide significant guidance and reference for the design of nanophotonic devices, facilitating the exploration and realization of advanced optical functionalities.

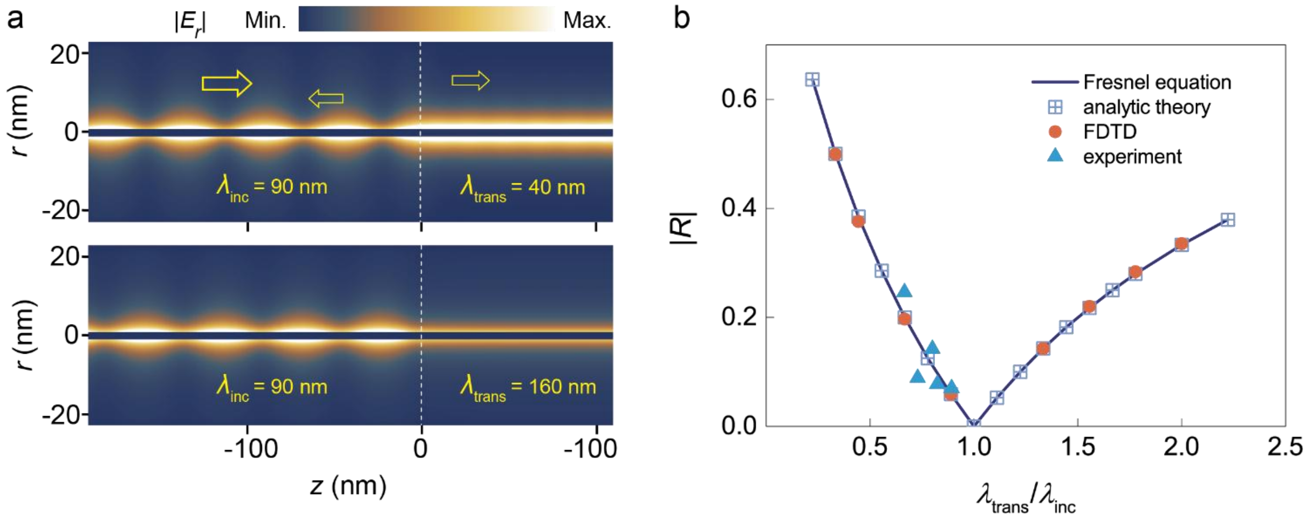

Figure 5. Theoretical analysis of the reflection of 1D plasmons at a junction. (a) Field maps of 1D plasmon amplitudes obtained numerically using the Finite-Difference Time-Domain (FDTD) method, illustrating two exemplary cases: $\lambda_{inc} > \lambda_{trans}$ and $\lambda_{inc} < \lambda_{trans}$, where λ_{inc} and λ_{trans} denote the plasmon wavelengths in the metallic and semiconducting regions, respectively. White dashed lines indicate the position of the junction. (b) Analytically and numerically calculated plasmon reflection amplitudes at junctions with different wavelengths of the transmitted plasmon wave (see SI for details).

We have designed and demonstrated, for the first time, nanoscale Luttinger-liquid FEPT devices crafted from metallic-semiconducting CNT junctions. These devices can efficiently manage the flow of plasmon waves through electrostatic gating, achieving nearly full transmission when activated and none when deactivated. Theoretical analysis and numerical simulations reveal that the 1D plasmon reflection and transmission at the junction align closely with the classical Fresnel equation, providing a valuable reference for the innovative design of nanoplasmonic devices. Thanks to the remarkable characteristics of the CNT plasmons—including strong spatial confinement, high quality factor, and the electrical tunability—the developed nanoscale FEPTs hold significant promise as essential components for advanced high-frequency nanophotonic circuits.

It's important to note that the reflectivity of plasmons at the metallic-semiconducting CNT junctions is determined solely by the ratio of the plasmon wavelengths on either side, independent of their absolute values. Consequently, the findings presented here for the far infrared at 10.6 μm are also applicable to the telecom wavelength range, provided that the field-effect plasmonic transistors are fabricated using small-diameter CNTs with bandgaps exceeding the telecom photon energy (~0.8 eV). This ensures a long lifetime and a high quality-factor for the telecom plasmons.

Moreover, the functional area of the developed FEPTs is extremely small, with a CNT diameter of just 1 to 2 nm and a junction length in the sub-nanometer range of a few benzene units[38]. Consequently, these carbon-based FEPTs can potentially be miniaturized to a few nanometers, making them comparable to or even smaller than current silicon-based electronic FETs.

References

1. Bohr, M. T., Nanotechnology goals and challenges for electronic applications. *IEEE Transactions on Nanotechnology* **2002,** *1* (1), 56-62.
2. Ballarini, D.; De Giorgi, M.; Cancellieri, E.; Houdré, R.; Giacobino, E.; Cingolani, R.; Bramati, A.; Gigli, G.; Sanvitto, D., All-optical polariton transistor. *Nature Communications* **2013,** *4* (1), 1778.
3. Miller, D. A. B., Are optical transistors the logical next step? *Nature Photonics* **2010,** *4* (1), 3-5.
4. Ríos, C.; Stegmaier, M.; Hosseini, P.; Wang, D.; Scherer, T.; Wright, C. D.; Bhaskaran, H.; Pernice, W. H. P., Integrated all-photonic non-volatile multi-level memory. *Nature Photonics* **2015,** *9* (11), 725-732.
5. Nozaki, K.; Tanabe, T.; Shinya, A.; Matsuo, S.; Sato, T.; Taniyama, H.; Notomi, M., Sub-femtojoule all-optical switching using a photonic-crystal nanocavity. *Nature Photonics* **2010,** *4* (7), 477-483.
6. Almeida, V. R.; Barrios, C. A.; Panepucci, R. R.; Lipson, M., All-optical control of light on a silicon chip. *Nature* **2004,** *431* (7012), 1081-1084.
7. Sun, C.; Wade, M. T.; Lee, Y.; Orcutt, J. S.; Alloatti, L.; Georgas, M. S.; Waterman, A. S.; Shainline, J. M.; Avizienis, R. R.; Lin, S.; Moss, B. R.; Kumar, R.; Pavanello, F.; Atabaki, A. H.; Cook, H. M.; Ou, A. J.; Leu, J. C.; Chen, Y.-H.; Asanović, K.; Ram, R. J.; Popović, M. A.; Stojanović, V. M., Single-chip microprocessor that communicates directly using light. *Nature* **2015,** *528* (7583), 534-538.
8. Zhang, Y.; Wang, Y.; Dai, Y.; Bai, X.; Hu, X.; Du, L.; Hu, H.; Yang, X.; Li, D.; Dai, Q.; Hasan, T.; Sun, Z., Chirality logic gates. *Science Advances* **2022,** *8* (49), eabq8246.
9. Barnes, W. L.; Dereux, A.; Ebbesen, T. W., Surface plasmon subwavelength optics. *Nature* **2003,** *424* (6950), 824-830.
10. Pendry, J. B.; Aubry, A.; Smith, D. R.; Maier, S. A., Transformation Optics and Subwavelength Control of Light. *Science* **2012,** *337* (6094), 549-552.
11. Gramotnev, D. K.; Bozhevolnyi, S. I., Plasmonics beyond the diffraction limit. *Nature Photonics* **2010,** *4* (2), 83-91.
12. Low, T.; Chaves, A.; Caldwell, J. D.; Kumar, A.; Fang, N. X.; Avouris, P.; Heinz, T. F.; Guinea, F.; Martin-Moreno, L.; Koppens, F., Polaritons in layered two-dimensional materials. *Nature Materials* **2017,** *16* (2),

182-194.
13. Basov, D. N.; Fogler, M. M.; García de Abajo, F. J., Polaritons in van der Waals materials. *Science* **2016,** *354* (6309), aag1992.
14. Fei, Z.; Rodin, A. S.; Andreev, G. O.; Bao, W.; McLeod, A. S.; Wagner, M.; Zhang, L. M.; Zhao, Z.; Thiemens, M.; Dominguez, G.; Fogler, M. M.; Neto, A. H. C.; Lau, C. N.; Keilmann, F.; Basov, D. N., Gate-tuning of graphene plasmons revealed by infrared nano-imaging. *Nature* **2012,** *487* (7405), 82-85.
15. Chen, J.; Badioli, M.; Alonso-González, P.; Thongrattanasiri, S.; Huth, F.; Osmond, J.; Spasenović, M.; Centeno, A.; Pesquera, A.; Godignon, P.; Zurutuza Elorza, A.; Camara, N.; de Abajo, F. J. G.; Hillenbrand, R.; Koppens, F. H. L., Optical nano-imaging of gate-tunable graphene plasmons. *Nature* **2012,** *487* (7405), 77-81.
16. Pogna, E. A. A.; Pistore, V.; Viti, L.; Li, L.; Davies, A. G.; Linfield, E. H.; Vitiello, M. S., Near-field detection of gate-tunable anisotropic plasmon polaritons in black phosphorus at terahertz frequencies. *Nature Communications* **2024,** *15* (1), 2373.
17. Yao, B.; Liu, Y.; Huang, S.-W.; Choi, C.; Xie, Z.; Flor Flores, J.; Wu, Y.; Yu, M.; Kwong, D.-L.; Huang, Y.; Rao, Y.; Duan, X.; Wong, C. W., Broadband gate-tunable terahertz plasmons in graphene heterostructures. *Nature Photonics* **2018,** *12* (1), 22-28.
18. Ni, G. X.; McLeod, A. S.; Sun, Z.; Wang, L.; Xiong, L.; Post, K. W.; Sunku, S. S.; Jiang, B. Y.; Hone, J.; Dean, C. R.; Fogler, M. M.; Basov, D. N., Fundamental limits to graphene plasmonics. *Nature* **2018,** *557* (7706), 530-533.
19. Sanders, A. W.; Routenberg, D. A.; Wiley, B. J.; Xia, Y.; Dufresne, E. R.; Reed, M. A., Observation of Plasmon Propagation, Redirection, and Fan-Out in Silver Nanowires. *Nano Letters* **2006,** *6* (8), 1822-1826.
20. Chen, X.-W.; Sandoghdar, V.; Agio, M., Highly Efficient Interfacing of Guided Plasmons and Photons in Nanowires. *Nano Letters* **2009,** *9* (11), 3756-3761.
21. Ditlbacher, H.; Hohenau, A.; Wagner, D.; Kreibig, U.; Rogers, M.; Hofer, F.; Aussenegg, F. R.; Krenn, J. R., Silver Nanowires as Surface Plasmon Resonators. *Physical Review Letters* **2005,** *95* (25), 257403.
22. Wang, S.; Wu, F.; Watanabe, K.; Taniguchi, T.; Zhou, C.; Wang, F., Metallic Carbon Nanotube Nanocavities as Ultracompact and Low-loss Fabry–Perot Plasmonic Resonators. *Nano Letters* **2020,** *20* (4), 2695-2702.
23. Shi, Z.; Hong, X.; Bechtel, H. A.; Zeng, B.; Martin, M. C.; Watanabe, K.; Taniguchi, T.; Shen, Y.-R.; Wang, F., Observation of a Luttinger-liquid plasmon in metallic single-walled carbon nanotubes. *Nature Photonics* **2015,** *9* (8), 515-519.
24. Wang, S.; Zhao, S.; Shi, Z.; Wu, F.; Zhao, Z.; Jiang, L.; Watanabe, K.; Taniguchi, T.; Zettl, A.; Zhou, C.; Wang, F., Nonlinear Luttinger liquid plasmons in semiconducting single-walled carbon nanotubes. *Nature Materials* **2020,** *19* (9), 986-991.
25. Noginov, M. A.; Zhu, G.; Belgrave, A. M.; Bakker, R.; Shalaev, V. M.; Narimanov, E. E.; Stout, S.; Herz, E.; Suteewong, T.; Wiesner, U., Demonstration of a spaser-based nanolaser. *Nature* **2009,** *460* (7259), 1110-1112.
26. Park, S. H.; Sammon, M.; Mele, E.; Low, T., Plasmonic gain in current biased tilted Dirac nodes. *Nature Communications* **2022,** *13* (1), 7667.
27. Dionne, J. A.; Diest, K.; Sweatlock, L. A.; Atwater, H. A., PlasMOStor: A Metal−Oxide−Si Field Effect Plasmonic Modulator. *Nano Letters* **2009,** *9* (2), 897-902.
28. McPolin, C. P. T.; Olivier, N.; Bouillard, J.-S.; O'Connor, D.; Krasavin, A. V.; Dickson, W.; Wurtz, G. A.; Zayats, A. V., Universal switching of plasmonic signals using optical resonator modes. *Light: Science & Applications* **2017,** *6* (6), e16237-e16237.
29. Guo, X.; Liu, R.; Hu, D.; Hu, H.; Wei, Z.; Wang, R.; Dai, Y.; Cheng, Y.; Chen, K.; Liu, K.; Zhang, G.; Zhu, X.; Sun, Z.; Yang, X.; Dai, Q., Efficient All-Optical Plasmonic Modulators with Atomically Thin Van Der Waals

Heterostructures. *Advanced Materials* **2020,** *32* (11), 1907105.
30. Falk, A. L.; Koppens, F. H. L.; Yu, C. L.; Kang, K.; de Leon Snapp, N.; Akimov, A. V.; Jo, M.-H.; Lukin, M. D.; Park, H., Near-field electrical detection of optical plasmons and single-plasmon sources. *Nature Physics* **2009,** *5* (7), 475-479.
31. Neutens, P.; Van Dorpe, P.; De Vlaminck, I.; Lagae, L.; Borghs, G., Electrical detection of confined gap plasmons in metal–insulator–metal waveguides. *Nature Photonics* **2009,** *3* (5), 283-286.
32. Wang, S.; Wu, F.; Zhao, S.; Watanabe, K.; Taniguchi, T.; Zhou, C.; Wang, F., Logarithm Diameter Scaling and Carrier Density Independence of One-Dimensional Luttinger Liquid Plasmon. *Nano Letters* **2019,** *19* (4), 2360-2365.
33. Luo, X.; Hu, C.; Lyu, B.; Yang, L.; Zhou, X.; Deng, A.; Kang, J.-H.; Shi, Z., Reflection phase shift of one-dimensional plasmon polaritons in carbon nanotubes. *Physical Review B* **2020,** *101* (4), 041407.
34. Yao, Y.; Li, Q.; Zhang, J.; Liu, R.; Jiao, L.; Zhu, Y. T.; Liu, Z., Temperature-mediated growth of single-walled carbon-nanotube intramolecular junctions. *Nature Materials* **2007,** *6* (4), 283-286.
35. Yao, Y.; Dai, X.; Liu, R.; Zhang, J.; Liu, Z., Tuning the Diameter of Single-Walled Carbon Nanotubes by Temperature-Mediated Chemical Vapor Deposition. *The Journal of Physical Chemistry C* **2009,** *113* (30), 13051-13059.
36. White, C. T.; Mintmire, J. W., Fundamental Properties of Single-Wall Carbon Nanotubes. *The Journal of Physical Chemistry B* **2005,** *109* (1), 52-65.
37. Laird, E. A.; Kuemmeth, F.; Steele, G. A.; Grove-Rasmussen, K.; Nygård, J.; Flensberg, K.; Kouwenhoven, L. P., Quantum transport in carbon nanotubes. *Reviews of Modern Physics* **2015,** *87* (3), 703-764.
38. Yao, Z.; Postma, H. W. C.; Balents, L.; Dekker, C., Carbon nanotube intramolecular junctions. *Nature* **1999,** *402* (6759), 273-276.